2012-4-2

Regulation of Morphogenesis and Neural Differentiation of Human Mesenchymal Stem Cells Using Carbon Nanotube Sheets

Jeong Ah Kim, *et al.*

Integrative Biology

Quantitative biosciences from nano to macro

www.rsc.org/ibiology

Volume 4 | Number 6 | June 2012 | Pages 577–702

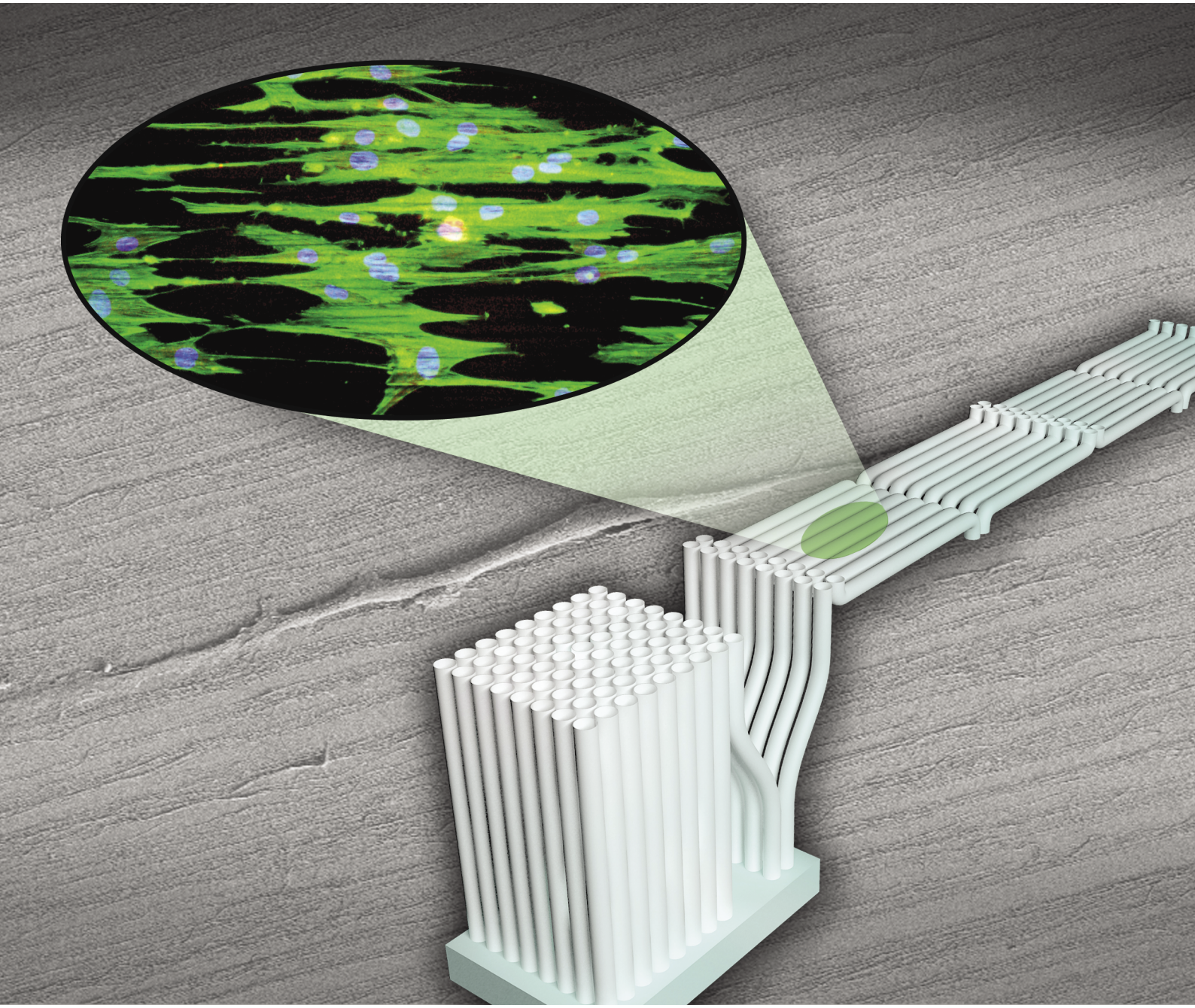

ISSN 1757-9694

RSC Publishing

PAPER

Park *et al.*

Regulation of morphogenesis and neural differentiation of human mesenchymal stem cells using carbon nanotube sheets

1757-9694(2012)4:6;1-P

Integrative Biology

Cite this: *Integr. Biol.*, 2012, **4**, 587–594

www.rsc.org/ibiology

PAPER

Regulation of morphogenesis and neural differentiation of human mesenchymal stem cells using carbon nanotube sheets†

Jeong Ah Kim,[a] Eui Yun Jang,[b] Tae June Kang,[b] Sungjun Yoon,[c] Raquel Ovalle-Robles,[d] Won Jong Rhee,[e] Taewoo Kim,[b] Ray H. Baughman,[d] Yong Hyup Kim[b] and Tai Hyun Park*[ac]

Received 1st February 2012, Accepted 29th March 2012
DOI: 10.1039/c2ib20017a

In order to successfully utilize stem cells for therapeutic applications in regenerative medicine, efficient differentiation into a specific cell lineage and guidance of axons in a desired direction is crucial. Here, we used aligned multi-walled carbon nanotube (MWCNT) sheets to differentiate human mesenchymal stem cells (hMSCs) into neural cells. Human MSCs present a preferential adhesion to aligned CNT sheets with longitudinal stretch parallel to the CNT orientation direction. Cell elongation was 2-fold higher than the control and most of the cells were aligned on CNT sheets within 5° from the CNT orientation direction. Furthermore, a significant, synergistic enhancement of neural differentiation was observed in hMSCs cultured on the CNT sheets. Axon outgrowth was also controlled using nanoscale patterning of CNTs. This CNT sheet provides a new cellular scaffold platform that can regulate morphogenesis and differentiation of stem cells, which could open up a new approach for tissue and stem cell regeneration.

Introduction

Regenerative therapeutics using stem cells has been a promising technique for the treatment of incurable neurological diseases including Parkinson's disease and spinal cord injury. Stem cells have multipotency to differentiate into specific lineages under different inducing conditions, making them a powerful tool for the regeneration of the biological function of injured tissues.[1,2] For these applications, it is crucial to efficiently transplant the stem cells into the specific target regions without any loss in blood flow or body fluid. In some cases, the transplanted stem cells must be aligned or oriented in a desired direction.[3] For example, neural cells should be synaptically connected with neural networks between cells for electrical signal transfer.[3–5] Therefore, it is important to ensure both complete neural induction and morphological guidance of neurite outgrowth of cells to facilitate the formation of an effective neural network and regeneration.[6,7]

In order to control proliferation, differentiation and orientation of cells, topographical and biochemical cues using nanotechnology have been utilized.[6,8] Traditionally, in order to position and

[a] *School of Chemical & Biological Engineering, Bio-Max Institute, Seoul National University, 599 Daehakdong, Gwanak-gu, Seoul 151-744, Republic of Korea. E-mail: thpark@snu.ac.kr; Fax: +82-2-875-9348; Tel: +82-2-880-8020*
[b] *School of Mechanical & Aerospace Engineering, Institute of Advanced Aerospace Technology, Seoul National University, 599 Daehakdong, Gwanak-gu, Seoul 151-744, Republic of Korea*
[c] *Interdisciplinary Program of Bioengineering, Seoul National University, 599 Daehakdong, Gwanak-gu, Seoul 151-744, Republic of Korea*
[d] *Alan G. McaDiarmid NanoTech Institute, University of Texas at Dallas, Richardson, TX 75083-0688, USA*
[e] *Division of Bioengineering, University of Incheon, 119 Academy-ro, Yeonsu-gu, Incheon 406-772, Republic of Korea*

† Electronic supplementary information (ESI) available: AFM data and primer sequences for RT-PCR. See DOI: 10.1039/c2ib20017a

Insight, innovation, integration

Aligned multi-walled carbon nanotube (MWCNT) sheets for the regulation of differentiation and directional nerve growth of human mesenchymal stem cells (hMSCs) are herein reported. In order to improve the efficient differentiation into a neural lineage and directional nerve growth, we used aligned MWCNT sheets as a neuro-regenerative matrix that are oriented in one in-plane direction and they aligned cells along a specific orientation. More interestingly, a synergistic enhancement of neural differentiation was observed in hMSCs cultured on the CNT sheet, even under non-neurogenic conditions. We also fabricated a multi-directional CNT sheet layer to assess cell migration and axon guidance on this matrix. This CNT sheet provides a scaffold platform that can regulate morphogenesis and differentiation of stem cells, which could allow new insight into the field of tissue and stem cell regeneration.

align cells, micro and nanoscale grooves or cavities were fabricated on a substrate providing contact guidance or patterning of cells with micro-scale resolution.[9–12] In addition, patterning of peptides or proteins[13–17] and biocompatible polymers[18,19] using soft lithography techniques has also been used to create a desired cell pattern. Moreover, a number of scaffolds have been suggested to control cell adhesion, migration, proliferation, and differentiation for tissue engineering.[7,20]

Despite the unique abilities of cell patterning techniques, there are still some limitations in creating three-dimensional structures that mimic the extracellular matrix (ECM). Recently, a variety of nanomaterials including nanoparticles,[21–23] carbon nanotubes,[3,24] nanofibers,[3,25,26] and nanoscale-substrates[27,28] were suggested for the transplantation and control of stem cell behavior. These nanoscale-engineered substrates and scaffolds can create appropriate extracellular environments and are biologically active due to their ability to interact with cellular molecules.[9,29,30] Because of these advantages, nanoscale materials can be used to efficiently control dynamic cellular behavior such as cell growth, migration and differentiation. In particular, carbon nanotubes (CNTs) have attracted increasing attention for use in biological applications because of their mechanical and electrical properties.[31,32] In addition, CNTs can be easily fabricated and functionalized.[33] For example, CNTs were used to reinforce scaffolds for cell implantation. Moreover, CNTs have been shown to improve the electrical properties of the substrates, and hence can increase the synaptic current or firing activity of neurons.[4,5,7,34]

In this study, we demonstrated that aligned CNT sheets can regulate the morphogenesis and differentiation of stem cells. The CNT sheet, comprising CNTs that are oriented in one in-plane direction, aligns cells along this specific orientation and manipulates cell behaviors by changing cell morphology and adhesion. We also investigated whether the expression levels of neural differentiated cells were influenced by these CNT sheets. Furthermore, we fabricated a multi-directional CNT sheet layer to assess cell migration and axon guidance on this matrix.

Materials and methods

Preparation of aligned CNT substrates

Vertically-aligned MWCNT arrays were grown on an iron-catalyst-coated silicon substrate by chemical vapor deposition of acetylene gas.[35] The as-grown MWCNT(s) were 8 to 15 nm in diameter and 150 to 180 μm in length. Using a sharp blade to start the process, the CNT sheets were drawn from the sidewall of a carbon nanotube forest at $\sim$3 cm s^{-1}. The direction of draw was orthogonal to the axis of the nanotubes in forest, as shown in Fig. 1A. Using this process, MWCNT(s) were self-assembled in a sheet-form and self-aligned in the draw direction. The CNT sheet typically has a density of $\sim$1.5 mg cm^{-3}, an areal density in the sheet plane of $\sim$1 to $\sim$3 μg cm^{-2}. The as-produced CNT sheets[36] were placed onto a 12 mm diameter cover glass. In order to fix the CNT sheet on the glass surface, ethanol was directly dropped onto the CNT sheet, followed by drying under ambient conditions. Details on the method used to produce the CNT sheets were described previously.[35,36]

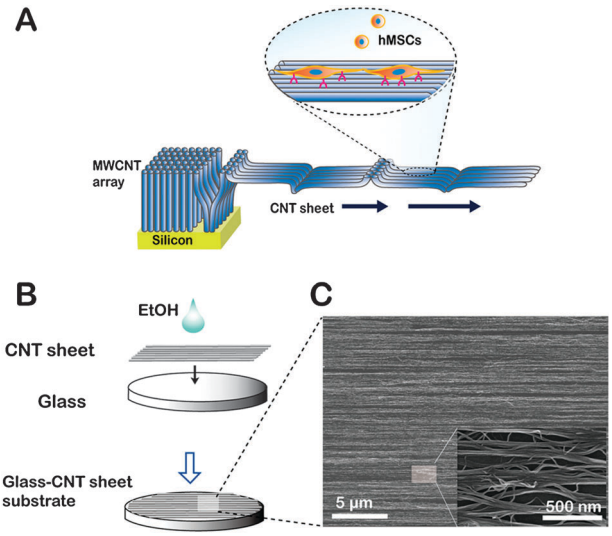

Fig. 1 (A) Schematic diagram of the fabrication of CNT sheets for culture with hMSCs. (B) Fabrication of the CNT–glass substrate using the drop-drying ethanol solvent method. (C) SEM images of CNT sheets. The inset provides a magnified image of the CNT bundle array. Magnification was 500× and 100 000× (inset image), respectively. The representation of the sheet draw process in (A) ignores the randomization of nanotube end location, which provides substantial uniformity in sheet structure along the sheet draw direction.

The amount of residual iron catalyst in the MWCNT sheets was less than 2 wt%.

Measurement of roughness and surface area of the CNT substrate and bare cover glass

The topography of the prepared CNT substrate and bare cover glass was investigated using an atomic force microscope (XE-159, PSIA co.). A 5 μm × 5 μm area was scanned for all substrates using non-contact mode. The roughness and surface area were calculated using an image processing program (XEI software).

Preparation of human mesenchymal stem cells (hMSCs)

Bone marrow-derived human MSCs (BM-MSCs) were purchased from Lonza (Switzerland). Cells were grown in 25 cm^2 tissue culture flasks containing nonhematopoietic (NH) expansion medium (Miltenyi Biotec GmbH, Germany) at 37 °C in a humidified CO_2 incubator. The cells were maintained until the confluency reached 90%, detached with trypsin-EDTA (Sigma, USA) and re-seeded for passage. To prevent the loss of differentiation potency following subsequent passages, the hMSCs were used only from passages 1–5.

Neural differentiation of hMSCs

For neural differentiation of hMSCs, cells were seeded into culture flasks containing NH expansion media at a cell density of 10 000 cells per cm^2. After cells completely adhered onto the flask, the culture media were changed with neurogenic media[37] containing forskolin (10 μM, Sigma), butylated hydroxyanisole (200 μM, Sigma), potassium chloride (5 mM, Sigma), valproic acid (2 mM, Sigma), hydrocortisone (1 μM, Sigma),

and insulin (5 μg ml^{-1}, Sigma) in DMEM/F12 media (Invitrogen, USA).

Immunofluorescence analysis

To visualize the hMSCs on the CNT sheets, hMSCs were immunostained against anti-β1-integrin and anti-β3-tubulin antibodies. After attachment, cells were fixed with Karnovsky's fixative (2% glutaraldehyde and 2% paraformaldehyde in 0.05 M sodium cacodylate buffer, pH 7.2) for 15 min and then permeabilized with 0.25% Triton X-100 diluted in PBS for 5 min. Cells were incubated for 2 h in a 1 : 250 dilution of primary antibody contained in blocking buffer (1% BSA in PBS with 0.25% Triton X-100) and washed 3 times with washing buffer (PBS with 0.25% Tween-20). The cells were then incubated for 2 h in a 1 : 250 dilution of Cy2-conjugated secondary antibody (Invitrogen, USA) and Alexa-fluor-548-conjugated secondary antibody (Invitrogen, USA) contained in 5% BSA blocking buffer. F-actin was stained with Alexa-fluor-488-phalloidin and the nucleus was counterstained with Hoechst 33342 for 15 min. After rinsing the cells with washing buffer, fluorescent images were taken using a fluorescence microscope (Olympus IX71, Japan).

Measurement of cell elongation and orientation

To assess morphological changes of hMSCs, immuno-fluorescence images of hMSCs cultured on substrates were analyzed using image analysis software (AnalySIS TS, Olympus, Japan). The magnitude of cell elongation was investigated based on the aspect ratio (major axis/minor axis) of the cells from three random captured images (n = 65–75 cells per group, triplicate). The orientation angle was also measured from the same images. The orientation angle was calculated based on the angle of the cells relative to the base line (horizontal line for the glass substrate, and parallel line to the CNT direction for the CNT sheet).

Adhesion assay

Prior to seeding the cells, the CNT–glass substrate and bare cover glass were placed into the 24-well plates and the surface of each substrate was blocked with blocking buffer (0.5% BSA in DMEM) at 37 °C in a CO_2 incubator for 1 h and then washed with washing buffer (0.1% BSA in DMEM). Cells were seeded in the wells at a concentration of 20 000 cells per well. After incubation in a CO_2 incubator for 15–120 min, the plates were shaken with 1500 rpm for 20 s. Plates were washed 2 times with washing buffer to remove detached cells and the adhered cells were fixed with 4% paraformaldehyde in PBS at room temperature for 20 min and washed with PBS. Finally, fixed cells were stained with crystal violet (5 mg ml^{-1} in 2% ethanol) and washed with water 3 times. Plates were completely dried and the cells were solubilized with 2% SDS in distilled water. The absorbance of the solubilized crystal violet was measured at 560 nm using an ELISA reader.

RT-PCR analysis

To quantify changes in the mRNA level of neural specific markers and adhesion molecules in hMSCs on CNT sheets, reverse transcription-polymerase chain reaction (RT-PCR) was carried out. RNA extraction was performed using TRIzol (Invitrogen, USA). RNA pellets were dissolved in RNase-free water, and RNA yields were measured using NanoDrop (Thermo scientific, USA). Total RNA (200–500 ng) was reverse-transcribed (Omniscript, Qiagen, Germany), and 1 μl of cDNA was used for PCR (35 cycles). The primers used for PCR are listed in Table S1 (ESI†). To examine the level of adhesion molecule, β1- and α5-integrin were used. To investigate changes in neural specific markers, β3-tubulin, microtubule element; NSE, neuron-specific enolase, which is found in mature neuron cells; GAP43, which is a crucial component of the axon and presynaptic terminal; NFL, neurofilament-light, which is important for the axon growth; MAP1b, microtubule-associated protein, which is essential in neurogenesis; and MAP2, microtubule-associated protein were used. GAPDH was used as a standard control.

Immunoblotting assay

An immunoblotting assay was performed to examine the expression level of β1-integrin in hMSCs cultured on CNT sheets. Total cell lysate was prepared using RIPA lysis buffer (25 mM Tris-HCl (pH 7.4), 150 mM NaCl, 1% Triton X-100, 1% sodium deoxycholate, 0.1% SDS, and 1% protease inhibitor cocktail), followed by centrifugation. The BCA assay was used to quantify total protein in the cell lysate, and the same amount of protein samples was loaded on the gel (10% polyacrylamide gel). After SDS-PAGE, the proteins were electro-transferred (90 min, 0.12 A) to a nitrocellulose membrane (Whatman GmbH, Germany). After the membrane was blocked with blocking buffer (0.1% Tween 20, and 5% skim milk in PBS, pH 7.4) for 90 min, the membrane was incubated overnight at 4 °C with anti-β1-integrin and anti-GAPDH primary antibodies diluted in blocking buffer (0.1% Tween 20, and 1% skim milk in PBS, pH 7.4) to 1 : 1000 (v/v). After washing (0.1% Tween 20 in PBS, pH 7.4), the membrane was incubated for 2 h at room temperature with a 1 : 1000 (v/v) dilution of HRP-conjugated secondary antibodies. After washing the membrane, labeled proteins were visualized using the ECL detecting solution (Calbiochem, USA) and was analyzed using an image analysis system (Syngene, UK).

Scanning electron microscopy

Human MSCs cultured on aligned CNT sheets were imaged by SEM. Cells were seeded on the CNT–glass substrate and differentiated into neuron under neurogenic conditions. After fixation with 2% (w/v) glutaraldehyde and 2% (w/v) para-formaldehyde in 0.05 M sodium cacodylate buffer for 30 min at 4 °C, cells were dehydrated in an ascending series of ethanol (30%, 40%, 50%, 70%, 80%, 90%, and 100%). Finally, cells were immersed in HMDS (hexamethyldisilazane) for 5 min and completely dried. After Pt sputter-coating, the cell morphology was observed using a field emission scanning electron micro-scope (FE-SEM, Carl Zeiss, Germany). The acceleration voltage was 2.0 kV and the magnification was 1000×.

Statistical analysis

Elongation, orientation, adhesion assay, and RT-PCR analysis were performed in triplicate experiments and compared with the control. Other experiments were performed using multiple experiments. A t-test was performed and $p < 0.05$ was considered to be statistically significant.

Results

CNT sheets for the culture of hMSCs were produced from the vertically aligned MWCNT array, which was synthesized by catalytic vapor deposition, as schematically illustrated in Fig. 1A. Details on CNT sheet fabrication were described previously.[35,36] The produced CNT sheet was placed onto a cover glass and then strongly adhered to the glass surface using the drop-drying ethanol solvent method (Fig. 1B). As ethanol evaporated, the CNT sheet densified to a thickness of about 50 nm. Fabricated CNT sheets were observed by SEM as shown in Fig. 1C. The CNT sheet was comprised of CNT bundles having a diameter of several tens of nanometres. The bundle arrays contain nanoscale and microscale pores, and have local deviation from alignment that does not propagate to a longer dimensional scale (Fig. 1C).

AFM analysis was performed to observe the topography of the fabricated CNT–glass substrate (see ESI†, Fig. S1). Nanoscale features were distributed non-uniformly and the height of the features ranged from 0 to 50 nm (Fig. S1A, ESI†). Surface topology and roughness were also examined for a 5 μm × 5 μm substrate area. The overall roughness (R_{rms}) of the CNT sheet was about 32–36 nm, whereas that of cover glass was less than 5 nm (Fig. S1B, ESI†), which indicates that the cover glass was relatively smooth and the CNT sheet was relatively rough with nanoscale features. The surface area was calculated from the AFM images. Consequently, the constructed CNT substrate had the topographical structures that increased its overall surface area.

To investigate the cellular response to the nanoscale structure of the CNT sheet, human mesenchymal stem cells (hMSCs) were seeded onto the CNT sheet. After incubating the hMSCs on the substrate for 24 h, cells were stained with phalloidin (for staining F-actin), anti-β1-integrin antibody, and Hoechst (for staining nucleus) to more clearly visualize the structures and orientation of the cells. Cells adhered on the cover glass had no determined orientation, whereas for the CNT sheet, most cells were elongated and grew in an orientation that was in the parallel direction of the CNTs (Fig. 2). To examine the elongation and orientation of the cells, the aspect ratio

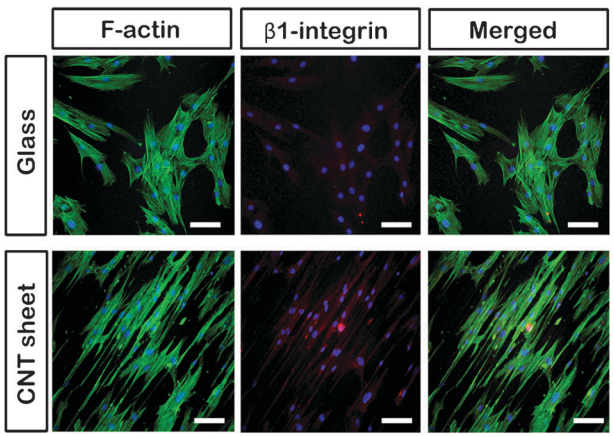

Fig. 2 Immunofluorescence images of hMSCs on glass and CNT sheet. After incubation under expansion conditions for 24 h, cells were treated with Alexa-fluor-488 phalloidin, anti-β1-integrin antibody (primary), and Hoechst (green: F-actin; red: β1-integrin; blue: nucleus). Scale bars are 100 μm.

(major axis to minor axis of cell body) and the angle of cells relative to the base line were measured, as illustrated in Fig. 3A. The aspect ratio was higher than 10 for cells grown on the CNT sheet, which was 2-fold higher than the cells grown on the smooth surface (Fig. 3B). The angle of the cells relative to the base line also deviated less on the CNT sheet. The base line was defined as a parallel line to the CNTs for the case of the CNT sheet, and an arbitrary horizontal line for the case of glass. The hMSCs had fibroblast-like morphologies on the cover glass without any specific orientation (35° ± 25°). In contrast, the deviation angle for cells on the CNT sheet was less than 5°, indicating that the cells were well-oriented along the direction of the CNTs (Fig. 3C). This result demonstrates that the nanotopographical cues of the CNTs guided the position of attachment and controlled cell morphologies. Interestingly, the nuclear shape was also dramatically changed from round shape to elongated when grown on the aligned sheet pattern and the deformation of nucleus was about 1.5-fold higher on the CNT sheet than on the smooth glass (Fig. 3D).

To investigate the effect of the nanostructure of the CNT sheet on cell differentiation, hMSCs were induced to differentiate into neural cells on the CNT sheet under neurogenic conditions. Differentiated cells were observed after immunostaining the neural maker, β3-tubulin. During differentiation into neurons, the cell adopted a sharp morphology and several neurites were observed. As shown in Fig. 4A, the cell body and neurites were also elongated and oriented on the CNT sheet. SEM analysis was used to observe the interaction between the cell and substrate. In this analysis, both the cell body and neurites were found to be stretched out and aligned along the CNTs (Fig. 4B). To quantitatively assess the effect of substrate topology on cell differentiation, the expression level of neural markers in hMSCs on the CNT sheet was measured. Six representative neural markers were selected and are listed in Table S1 (see ESI†). Most of the neural markers were upregulated in the CNT sheet when compared to the cover glass although the level of increase was different (Fig. 5). Interestingly, the expression levels of some of the neural markers were enhanced even under the non-neurogenic conditions by only culturing the cells on the CNT sheet. As shown in Fig. 2 and 3, the orientation of the CNT substrate affected cell elongation and orientation. It is likely that this effect also altered cell signaling cascades and promoted neural differentiation. However, under the neurogenic conditions, upregulation of the neural markers was higher than under the non-neurogenic conditions.

The shape of the cells adhered to the substrate is generally changed through the interaction with the topological pattern. Because cell adhesion to the substrate influences the interaction between the cytoskeleton and adhesion protein,[6,29,30] the initial cell attachment on the topological pattern can further accelerate cellular functions such as differentiation and migration. It is also noticed in Fig. 2 that the fluorescence of β1-integrin was brighter in the cells grown on the CNT sheets than cells grown on glass indicating upregulated adhesion proteins on CNTs. To investigate the effect of CNTs on hMSC attachment, cells in the early stage (within 120 min) of the cultivation were analyzed (Fig. 6A). CNT–glass and cover glass substrates were coated with BSA to make them unfavorable for the attachment of cells and then the cells were

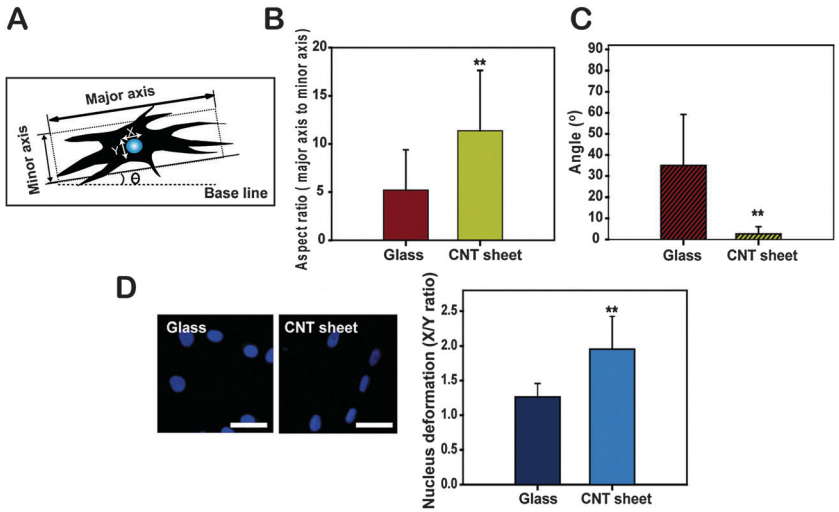

Fig. 3 Elongation and orientation of hMSCs on the glass and CNT sheet. (A) Illustration of the method used to measure elongation and orientation. (B) The aspect ratio (major axis to minor axis of cell body) was obtained from the three random captured images (number of cells, glass: $n = 65$; CNT sheet: 75). (C) The orientation angle of the cells relative to the base line was measured, where the base line was an arbitrary horizontal line for the glass and a parallel line to CNTs for the CNT sheet. (Number of cells, glass: $n = 57$; CNT sheet: 62.) (D) Nucleus shape was also elongated on the CNT sheet (left) and the deformation level of the nucleus was measured (right). Scale bars are 50 μm. The asterisks (**) indicate statistically significant difference between glass and CNT sheets ($P < 0.00001$).

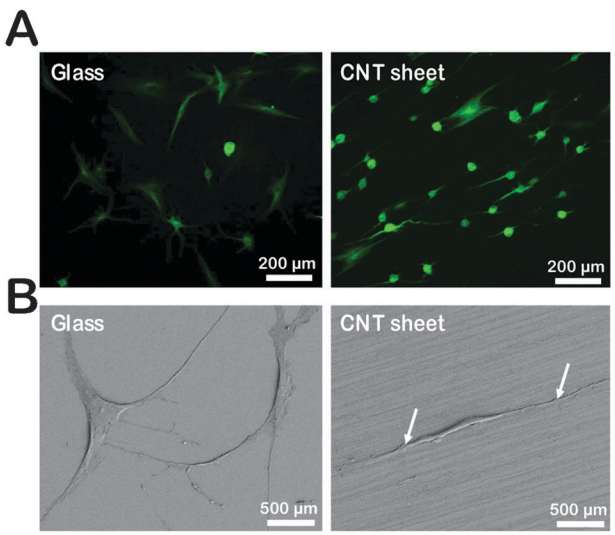

Fig. 4 Neural differentiation of hMSCs on the glass and CNT sheet substrates. Differentiation was induced 24 h after seeding. (A) Morphological changes in the cells were observed using immunostaining of β3-tubulin expressed in hMSCs (6 h after induction). (B) SEM images of differentiated hMSCs on the glass and CNT sheet (24 h after induction). White arrows indicate neurites adhered along the CNTs. Magnification was 1000×.

incubated on their substrates. Under this condition, cell adhesion was slightly faster on the CNT sheet than on the bare glass. Most of the cells were spherical and rarely attached to the glass surface within 120 min after seeding. In contrast, a majority of the cells had adhered and started to spread out on the surface within 120 min after seeding on the CNT sheet. The results of the adhesion assay also showed that the cells were more adhesive to the CNT substrate (Fig. 6B and C). For instance, after shaking cells adhered to substrates both on glass and on CNT sheets, for 20 seconds at 1500 rpm, the amount of remaining cells still adhered to the CNT sheets was higher than on the bare glass indicating a stronger cell adhesion to the CNT sheet. The amount of intracellular adhesion molecules was quantified and compared. Integrin–ligand interaction is essential to anchor the cell on the substrate, and it influences signal cascades related to cellular function. Using RT-PCR and immunoblotting assay, the level of adhesion markers, α5- and β1-integrin, was measured. In these experiments, the expression of the adhesion molecules was shown to be upregulated on the aligned CNT sheets (Fig. 6C and D). These data demonstrate that the expression of intracellular proteins relevant to cell–matrix interaction and adhesion was enhanced by the CNT sheet.

In neurodisease models of stem cell therapy, cellular behavior such as axonal outgrowth or migration is important. To observe the possibility of the direction control of axon outgrowth using the substrate topology of CNT sheets, a stack of two orthogonally oriented CNT sheets was constructed as shown in Fig. 7. The hMSCs were seeded on the CNT sheets and then differentiated into neural cells. Interestingly, in the region of intersection, cells recognized the pattern of the CNTs and turned the axons along the direction of the CNTs (Fig. 7A and B). In addition, cells adhered to the CNTs and their neurites stretched out along the CNTs. This indicates that the direction of neurite outgrowth can be controlled by the specific pattern of the CNTs. Therefore, CNT sheets can possibly be efficiently used for the regeneration and control of stem cells in tissue engineering applications.

Discussion

The combined results of this study clearly demonstrate that hMSCs preferentially adhere to the CNTs, allowing the cells to effectively differentiate into neural cells. This can be attributed to the roughness of CNTs caused by their nanoscale features.[12,30,38]

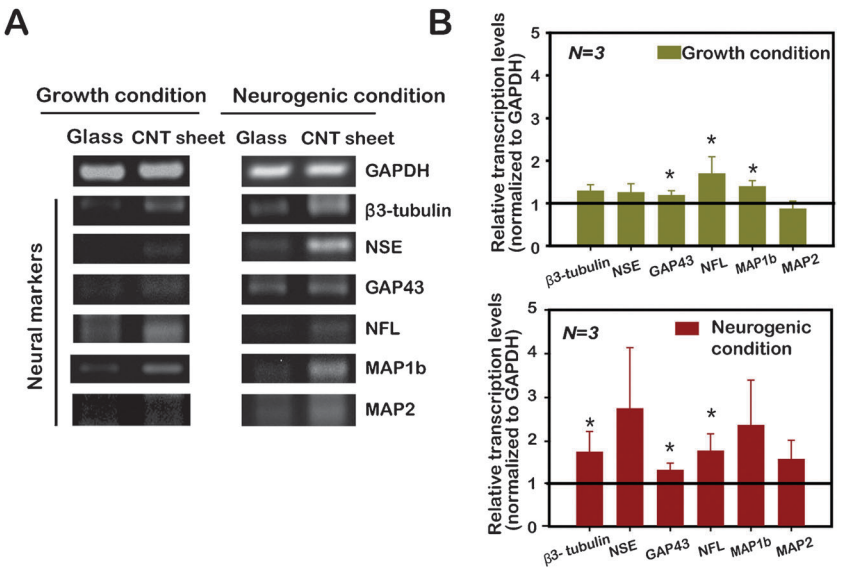

Fig. 5 (A) RT-PCR analysis of the expression of neural markers of hMSCs on the glass and CNT sheet. Cells were cultured under growth conditions or neurogenic conditions. After 24 h, mRNA was isolated from the harvested cells and PCR was performed using 35 cycles. Neural markers were upregulated in the CNT sheets under both growth and neurogenic conditions. (B) From the RT-PCR data, band intensity of each neural marker was measured and quantified from three independent experiments. The band intensity levels were relatively obtained compared to the level of glass (= 1). The asterisk (*) indicates statistically significant difference between glass and CNT sheets ($P < 0.05$).

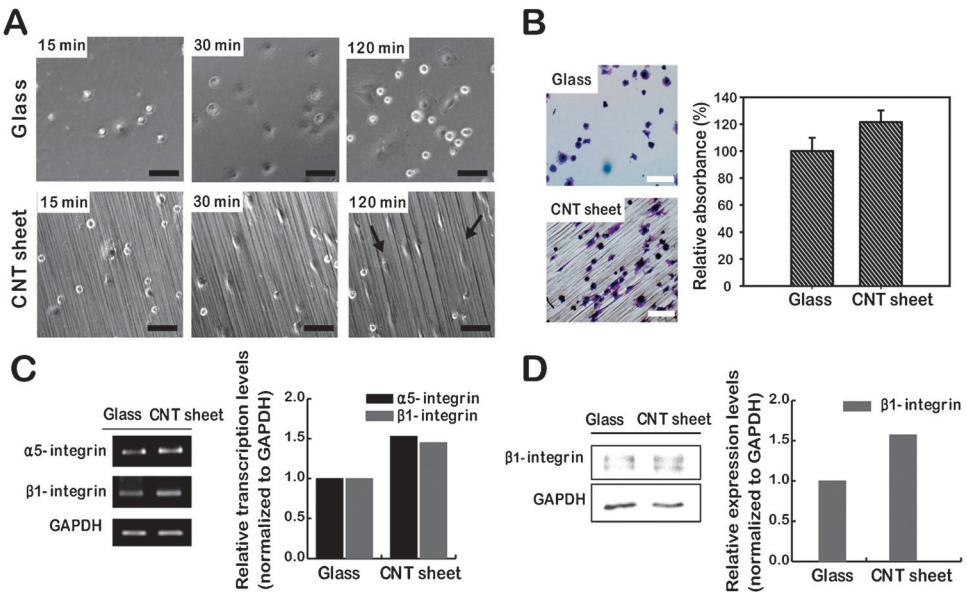

Fig. 6 Time course analysis of hMSC adhesion on the glass and CNT sheet substrates. (A) All images were representative images of cells observed at 15 min, 60 min, and 120 min, respectively, after seeding on the substrate under growth conditions. Black arrows represent attached and aligned cells on the sheet. Scale bars are 100 μm. (B) Quantitative analysis of hMSC adhesion on the glass and CNTs. Cells stained with crystal violet indicate remnant cells on the substrate after incubation (1 h) and subsequent shaking (1500 rpm, 20 s) (left). Scale bars are 100 μm. Relative absorbance of solubilized crystal violet was measured and quantified (right). (C) Quantitative RT-PCR analysis of the expression of adhesion molecules (α5-, β1-integrin), (D) immunoblotting assay of β1-integrin. The band intensity was normalized to GAPDH.

These nanoscale-features and topography provide cells anchorage sites for adhesion molecules and instructive clues to guide cell behavior.[38] The integrin receptors tether the cell cytoskeleton to the ECM and activate a cascade of intracellular signaling pathways where cellular behavior including adhesion, proliferation, migration, and differentiation is directly affected.[6,8] The general mechanism underlying the cellular response to nano-features is still largely unknown. In addition, surface topography, dimensions, conformation and symmetry of nanofeatures may also influence cellular responses.

It is also possible that the cell differentiation observed on the CNT sheets was caused by the change in the shape of the cell and nucleus. As shown in Fig. 2 and 3, the nucleus and cell shape was about 1.5-fold and 2-fold more elongated on the CNT sheets compared with that of control, respectively. Some studies have reported that cells grown on nano-textured

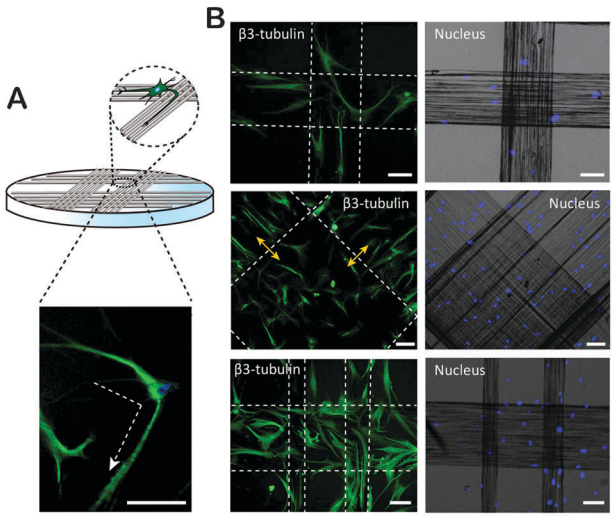

Fig. 7 Direction control of axon outgrowth of differentiated neural cells on a stack of two orthogonally oriented CNT sheets. (B) Cells were differentiated into neurons and tracked the CNT patterns. Cells were observed using immunostaining against β3-tubulin. Scale bars are 100 μm.

surfaces had an altered cell and nucleus shape, which might change the nuclear matrix protein and focal adhesion complexes and hence affect the expression of silent genes.[39] Modulating cell shape might be a critical factor in directing the fate of differentiation.[40–43] As shown in Fig. 5, the level of differentiation was higher on the CNT sheet than on glass. Therefore, increased adhesion as well as elongation may have synergistically affected cellular signaling pathways.

From above results, this MWCNT sheet has a potential to be used for the purpose of neural regeneration by implantation of neural cells cultured on this sheet for the enhancement of cell function and guidance of cell migration. The fabricated sheets may be too flexible to be implanted alone. However, CNT/gel or polymer hybrid structures which can robust this sheet would provide an efficient implantable material for the purpose of regeneration *in vivo*.

In spite of these tremendous potentials of CNTs, toxicity issue still remains to be clearly studied.[3,5] Some groups proved that MWCNTs were not toxic to cells,[44] but the other groups have reported results contradicting this.[45,46] If toxicity issue is overcome through further study, CNTs would provide an effective tool for therapeutic and regenerative use.

Conclusions

In conclusion, the nanoscale features of the CNT sheet enhanced cell focal adhesion by clustering integrin molecules and the topography of the CNTs changed the cell morphology and guided the orientation of the cells. This subsequently activated intracellular signaling cascades and enhanced differentiation. Although we do not clearly understand the precise mechanism of this process, the physical interaction between the cell and CNTs and parallel arrangement of the cells might enhance intracellular signaling. In addition to the flexible and favorable structure of the CNT for control over cell behavior, electrical stimulation of cells, which is a property of CNTs, would provide synergistic effects on regeneration of cell functions. Further studies are required to investigate the effect of electrical stimulation on cells using the engineered CNT sheet. The electrically effective and biocompatible three-dimensional materials would be useful to regenerate and guide neural cells. Therefore, the aligned- and nanofeatured CNT sheet holds great promise for use as a versatile technique in creating a three-dimensional culture matrix for stem cells and improving their therapeutic effects in regenerative medicine.

Acknowledgements

This work was supported by the Pioneer Research Program, the Basic Science Research Program, and National Nuclear R&D Program through the National Research Foundation of Korea (NRF) grant funded by the Ministry of Education, Science, and Technology (MEST) (No. 2011-0001643, 2011K000682 2011-0000331, 2011-0000318, 2011-0001293, and 2011-0018905).

Notes and references

1 Y. Jiang, B. N. Jahagirdar, R. L. Reinhardt, R. E. Schwartz, C. D. Keene, X. R. Ortiz-Gonzalez, M. Reyes, T. Lenvik, T. Lund, M. Blackstad, J. Du, S. Aldrich, A. Lisberg, W. C. Low, D. A. Largaespada and C. M. Verfaillie, *Nature*, 2002, **418**, 41–49.
2 M. F. Pittenger, A. M. Mackay, S. C. Beck, R. K. Jaiswal, R. Douglas, J. D. Mosca, M. A. Moorman, D. W. Simonetti, S. Craig and D. R. Marshak, *Science*, 1999, **284**, 143–147.
3 P. A. Tran, L. Zhang and T. J. Webster, *Adv. Drug Delivery Rev.*, 2009, **61**, 1097–1114.
4 V. Lovat, D. Pantarotto, L. Lagostena, B. Cacciari, M. Grandolfo, M. Righi, G. Spalluto, M. Prato and L. Ballerini, *Nano Lett.*, 2005, **5**, 1107–1110.
5 G. Cellot, E. Cilia, S. Cipollone, V. Rancic, A. Sucapane, S. Giordani, L. Gambazzi, H. Markram, M. Grandolfo, D. Scaini, F. Gelain, L. Casalis, M. Prato, M. Giugliano and L. Ballerini, *Nat. Nanotechnol.*, 2008, **4**, 126–133.
6 L. Ferreira, J. M. Karp, L. Nobre and R. Langer, *Cell Stem Cell*, 2008, **3**, 136–146.
7 S. Seidlits, J. Lee and C. Schmidt, *Nanomedicine*, 2008, **3**, 183–199.
8 N. J. Sniadecki, R. A. Desai, S. A. Ruiz and C. S. Chen, *Ann. Biomed. Eng.*, 2006, **34**, 59–74.
9 S.-J. Kim, J. K. Lee, J. W. Kim, J.-W. Jung, K. Seo, S.-B. Park, K.-H. Roh, S.-R. Lee, Y. H. Hong, S. J. Kim, Y.-S. Lee, S. J. Kim and K. S. Kang, *J. Mater. Sci.: Mater. Med.*, 2008, **19**, 2953–2962.
10 B. Zhu, Q. Lu, J. Yin, J. Hu and Z. Wang, *Tissue Eng.*, 2005, **11**, 825–834.
11 T. Peterbauer, S. Yakunin, J. Siegel, S. Hering, M. Fahrner, C. Romanin and J. Heitz, *J. Nanomater.*, 2011, **2011**, 413079.
12 X. Jiang, S. Takayama, X. Qian, E. Ostuni, H. Wu, N. Bowden, P. LeDuc, D. E. Ingber and G. M. Whitesides, *Langmuir*, 2002, **18**, 3273–3280.
13 M. A. Kafi, T.-H. Kim, J.-H. An and J.-W. Choi, *Biosens. Bioelectron.*, 2011, **26**, 3371–3375.
14 R. S. Kane, S. Takayama, E. Ostuni, D. E. Ingberb and G. M. Whitesides, *Biomaterials*, 2002, **23**, 161–166.
15 M. S. Hahn, J. S. Miller and J. L. West, *Adv. Mater.*, 2006, **18**, 2679–2684.
16 D. I. Rozkiewicz, Y. Kraan, M. W. T. Werten, F. A. de Wolf, V. Subramaniam, B. J. Ravoo and D. N. Reinhoudt, *Chem.–Eur. J.*, 2006, **12**, 6290–6297.
17 I. S. Carrico, S. A. Maskarinec, S. C. Heilshorn, M. L. Mock, J. C. Liu, P. J. Nowatzki, C. Franck, G. Ravichandran and D. A. Tirrell, *J. Am. Chem. Soc.*, 2007, **129**, 4874–4875.
18 M. Stevens, M. Mayer, D. G. Anderson, D. B. Weibel, G. M. Whitesides and R. Langer, *Biomaterials*, 2005, **26**, 7636–7641.
19 A. Khademhosseini, K. Y. Suh, J. M. Yang, G. Eng, J. Yeh, S. Levenberg and R. Langer, *Biomaterials*, 2004, **25**, 3583–3592.

20 J. P. Frampton, M. R. Hynd, M. L. Schuler and W. Shain, *Biomed. Mater.*, 2011, **6**, 015002.
21 E. E. Hui and S. N. Bhatia, *Langmuir*, 2007, **23**, 4103–4107.
22 D. S. Kommireddy, S. M. Sriram, Y. M. Lvov and D. K. Mills, *Biomaterials*, 2006, **27**, 4296–4303.
23 G. Frasca, F. Gazeau and C. Wilhelm, *Langmuir*, 2009, **25**, 2348.
24 B. S. Harrison and A. Atala, *Biomaterials*, 2007, **28**, 344–353.
25 E. Schnell, K. Klinkhammer, S. Balzer, G. Brook, D. Klee, P. Dalton and J. Mey, *Biomaterials*, 2007, **28**, 3012–3025.
26 A. F. Quigley, J. M. Razal, B. C. Thompson, S. E. Moulton, M. Kita, E. L. Kennedy, G. M. Clark, G. G. Wallace and R. M. Kapsa, *Adv. Mater.*, 2009, **21**, 4393–4397.
27 K. M. Woo, V. J. Chen and P. X. Ma, *J. Biomed. Mater. Res., Part A*, 2003, **67**, 531–537.
28 R. A. Brown, M. Wiseman, C. Chuo, U. Cheema and S. N. Nazhat, *Adv. Funct. Mater.*, 2005, **15**, 1762–1770.
29 J. Park, S. Bauer, K. von der Mark and P. Schmuki, *Nano Lett.*, 2007, **7**, 1686–1691.
30 X. Liu, J. Y. Lim, H. J. Donahue, R. Dhurjati, A. M. Mastro and E. A. Vogler, *Biomaterials*, 2007, **28**, 4535–4550.
31 E. B. Malarkey, K. A. Fisher, E. Bekyarova, W. Liu, R. C. Haddon and V. Parpura, *Nano Lett.*, 2009, **9**, 264–268.
32 M. Motta, Y.-L. Li, I. Kinloch and A. H. Windle, *Nano Lett.*, 2005, **5**, 1529–1533.
33 G. Bartholomeusz, P. Cherukuri, J. Kingston, L. Cognet, R. Lemos, T. K. Leeuw, L. Gumbiner-Russo, R. B. Weisman and G. Powis, *Nano Res.*, 2009, **2**, 279–291.
34 E. W. Keefer, B. R. Botterman, M. I. Romero, A. F. Rossi and G. W. Gross, *Nat. Nanotechnol.*, 2008, **3**, 434–439.
35 M. Zhang, K. R. Atkinson and R. H. Baughman, *Science*, 2004, **306**, 1358–1361.
36 M. Zhang, S. Fang, A. A. Zakhidov, S. B. Lee, A. E. Aliev, C. D. Williams, K. R. Atkinson and R. H. Baughman, *Science*, 2005, **309**, 1215–1219.
37 C. Y. Fong, M. Richards, N. Manasi, A. Biswas and A. Bongso, *Reprod. Biomed. Online*, 2007, **15**, 708–718.
38 E. K. F. Yim, S. W. Pang and K. W. Leong, *Exp. Cell Res.*, 2007, **313**, 1820–1829.
39 J. M. Dang and K. W. Leong, *Adv. Mater.*, 2007, **19**, 2775–2779.
40 M. J. Dalby, M. O. Riehle, S. J. Yarwood, C. D. Wilkinson and A. S. G. Curtis, *Exp. Cell Res.*, 2003, **284**, 272–280.
41 N. D. Relan, Y. Yang, S. Beqaj, J. H. Miner and L. Schuger, *J. Cell Biol.*, 1999, **147**, 1341–1350.
42 S. Beqaj, S. Jakkaraju, R. R. Mattingly, D. Pan and L. Schuger, *J. Cell Biol.*, 2002, **156**, 893–903.
43 S. Oh, K. S. Brammer, Y. S. J. Li, D. Teng, A. J. Engler, S. Chien and S. Jin, *Proc. Natl. Acad. Sci. U. S. A.*, 2009, **106**, 2130–2135.
44 A. O. Lobo, E. F. Antunes, A. H. A. Machado, C. Pacheco-Soares, V. J. Trava-airoldi and E. J. Corat, *Mater. Sci. Eng., C*, 2008, **28**, 264–469.
45 J. Muller, F. Huaux, N. Moreau, P. Misson, J.-F. Heilier, M. Delos, M. Arras, A. Fonseca, J. B. Nagy and D. Lison, *Toxicol. Appl. Pharmacol.*, 2005, **207**, 221–231.
46 A. Liu, K. Sun, J. Yang and D. Zhao, *J. Nanopart. Res.*, 2008, **10**, 1303–1307.

Electronic Supplementary Material (ESI) for Integrative Biology

Supplementary Information

Regulation of morphogenesis and neural differentiation of human mesenchymal stem cells using carbon nanotube sheets

Jeong Ah Kim,[a] *Eui Yun Jang,*[b] *Tae June Kang,*[b] *Sungjun Yoon,*[c] *Raquel Ovalle-Robles,*[d] *Won Jong Rhee,*[e] *Taewoo Kim,*[b] *Ray H. Baughman,*[d] *Yong Hyup Kim,*[b] *Tai Hyun Park,*[a,c,*]

[a]School of Chemical & Biological Engineering, Bio-Max Institute, Seoul National University, 599 Daehakdong, Gwanak-gu, Seoul 151-744, Republic of Korea

[b]School of Mechanical & Aerospace Engineering, Institute of Advanced Aerospace Technology, Seoul National University, 599 Daehakdong, Gwanak-gu, Seoul 151-744, Republic of Korea

[c]Interdisciplinary Program of Bioengineering, Seoul National University, 599 Daehakdong, Gwanak-gu, Seoul 151-744, Republic of Korea

[d]Alan G. McaDiarmid NanoTech Institute, University of Texas at Dallas, Richardson, TX 75083-0688, USA

[e]Biopharmaceutical R&D, LG Life Sciences, Ltd., 104-1, Munji-dong, Yuseong-gu, Daejeon 305-380, Republic of Korea

*Corresponding author. Email: thpark@snu.ac.kr (T. H. Park). Telephone: +82-2-880-8020. Fax: +82-2-875-9348.

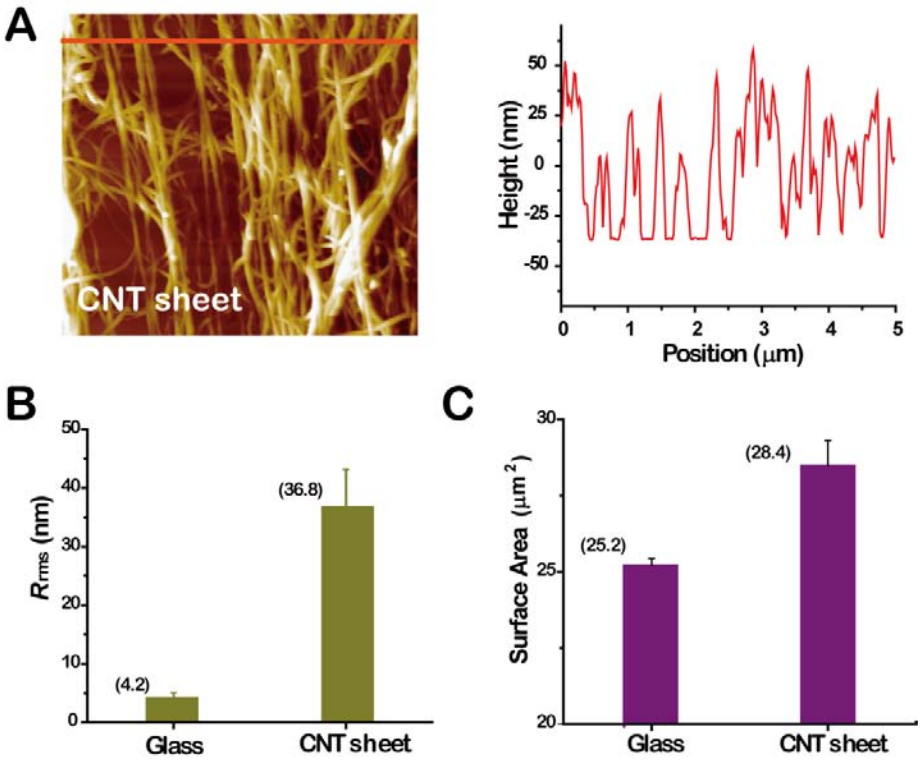

Figure S1. Surface characteristics of glass and CNT sheet using AFM. (A) Representative AFM image (left panel) and its line profile (right panel). A 5 μm × 5 μm area of each substrate was scanned and roughness (B) and surface area (C) were calculated.

Table S1. Primer sequence used in the RT-PCR analysis to determine the level of gene expression for cell adhesion (β1-and α5-integrin) and neural differentiation (β3-tubulin, NSE, GAP43, NFL, MAP1b, and MAP2). GAPDH was used as a standard control.

Marker	**Primer (forward)**	**Primer (reverse)**	**Size (bp)**	**Function**
β1-integrin	5'-CACTTTGCTGGAGATGGG-3'	5'-CCTACTGCTGACTTAGGG-3'	227	Adhesion, binding
α5-integrin	5'-CTGAAGATGCCCTACCGAAT-3'	5'-GGAGGGAGCGTTTGAAGAAT-3'	202	
β3-tubulin	5'-GGAACCATGGACAGTGTC-3'	5'-TTGCTGATGAGCAACGTGC-3'	251	Microtubule element
NSE	5'-TCTGTGGTGGAGCAAGAGAA-3'	5'-TGAGAGCCACCATTGATCAC-3'	217	Neuron-specific marker
GAP43	5'-GATGATGTCCAAGCTGCTGA-3'	5'-TTCTCCTCTGAGGATGCAG-3'	233	Component of axon and presynaps
NFL	5'-TTCCTTCAGCTACGAGCCGT-3'	5'CCAGACTGGGCATCAACGAT-3'	197	Axonal growth
MAP1b	5'-TGTCCTAGCAGCCAGTCAGT-3'	5'-CTCGAGGAGCTAAAATCAGC-3'	215	Microtubule assembly
MAP2	5'-TTCACGCACACCAGGCACT-3'	5'-GACATTCTTCAGGTCTGGCAG-3'	190	Microtubule-associated protein
GAPDH	5'-CCACTGGCGTCTTCACCA-3'	5'GCCAGGGGTGCTAAGCA-3'	190	Standard control